

444150

CAPTIONED BY DDC

AS AD NO.

Report No. 3
Third Quarterly Report

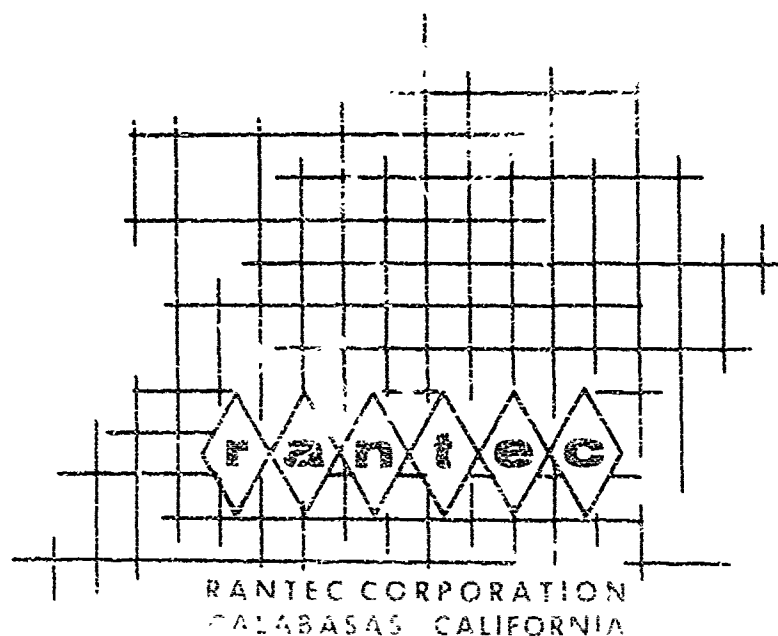
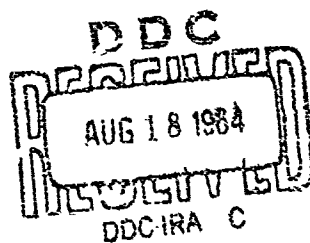
Covering the Period
1 January 1964 to 31 March 1964

**Investigation of
MICROWAVE DIELECTRIC-RESONATOR FILTERS**

Prepared for:
U. S. ARMY ELECTRONICS RESEARCH AND DEVELOPMENT LABORATORY
FORT MONMOUTH, NEW JERSEY

CONTRACT DA 36-039-AMC-02267(E)
TASK NO. 5544-PM-63-91

By: S. B. Cohn and K. C. Kelly



QUALIFIED REQUESTORS MAY OBTAIN COPIES OF THIS REPORT
DEFENSE DOCUMENTATION CENTER, CAMERON STATION, ALEXANDRIA, VIRGINIA.
D. D. C. RELEASE TO OTS NOT AUTHORIZED

Report No. 3
Third Quarterly Report

Covering the Period
1 January 1964 to 31 March 1964

**Investigation of
MICROWAVE DIELECTRIC-RESONATOR FILTERS**

Prepared for:

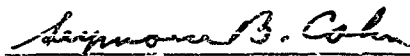
U. S. ARMY ELECTRONICS RESEARCH AND DEVELOPMENT LABORATORY
FORT MONMOUTH, NEW JERSEY

CONTRACT DA 36-059-AMC-02267(E)
TASK NO. 5544-PM-63-91

By: S. B. Cohn and K. C. Kelly

Rantec Project No. 31625

Approved:



SEYMOUR B. COHN, Technical Director

TABLE OF CONTENTS

SECTION	TITLE	PAGE
I	PURPOSE	1
II	ABSTRACT	2
III	CONFERENCES	4
IV	FACTUAL DATA	5
	Introduction	5
	Coupling Between Dielectric Resonators - Higher Modes	6
	Dielectric-Constant Measurements	16
	Measurement Error with the Circular- Waveguide Dielectrometer	16
	Measurement Error with the Radial- Waveguide Dielectrometer	19
	Anomalous Behavior of Sample Λ_2	19
	The Dielectric Constant of Cold Pressed Polycrystalline TiO_2 Pellets from USAERDL	20
	The Dielectric Constant of Eccoceram Hi-K90	21
	Temperature and Dielectric Constant	22
	Unloaded-Q and Center-Frequency Measurements	22
	Unloaded Q of TiO_2 Samples	22
	Q_u Versus Waveguide Dimensions	24
	f_o Versus Waveguide Dimensions	25
	Theoretical Analysis of f_o and Q_u	27
	Experiments with Two-Resonator Band-Pass Filters	27
V	CONCLUSIONS	33
VI	PROGRAM FOR NEXT INTERIM	33
VII	LIST OF REFERENCES	34
VIII	IDENTIFICATION OF KEY TECHNICAL PERSONNEL	35
	ASTIA CARDS	36

LIST OF ILLUSTRATIONS

FIGURE	TITLE	PAGE
2-1	Coupled Dielectric Resonators Inside a Rectangular Metal Tube	1
2-2	Coordinate System for Rectangular Waveguide . . .	10
2-3	Factor K, Ratio of Multiple-Mode Coupling-Coefficient Formula to Single-Mode Formula	16
2-4	Coupling-Coefficient Data for Configuration of Figure 2-1. Solid Curves from Single Mode Theory, Dotted Curve from Multi-Mode Theory, and Circled Points are Experimental	17
3-1	Density Vs. Dielectric Constant for USAERDI Cold Pressed TiO_2 Cylinders	21
3-2	Dielectric Constant Vs. Temperature (Temperature Coefficient in Brackets)	22
4-1	Q_u of Dielectric Resonator Vs. Dimension of Square Waveguide	25
4-2	f_0 of Dielectric Resonator Vs. Dimension of Square Waveguide	27
5-1	Maximally Flat Dielectric-Resonator Filter, $a = b = 0.750"$	28
5-2	Maximally Flat Dielectric-Resonator Filter, $a = b = 0.995"$	28

LIST OF TABLES

TABLE	TITLE	PAGE
4-1	Unloaded Q of Various TiO_2 Ceramic Disks	24

SECTION I

PURPOSE

This program is intended to study the feasibility of high-dielectric-constant materials as resonators in microwave filters, and to obtain design information for such filters. Resonator materials shall be selected that have loss tangents capable of yielding unloaded Q values comparable to that of waveguide cavities. The materials shall have dielectric constants of at least 75 in order that substantial size reductions can be achieved compared to the dimensions of waveguide filters having the same electrical performance.

SECTION II

ABSTRACT

The coupling-coefficient formula derived in the Second Quarterly Report is discussed. Its discrepancy from experimental data for close spacing is attributed to the use of only the TE_{10} mode in the analysis. The derivation is then extended to include all higher TE and TM modes excited by the dielectric resonators. The solution is particularized for dielectric disks spaced along the centerline of a rectangular waveguide below cutoff, with the axes of the disks parallel to the transverse x coordinate. Coupling-coefficient curves computed from the new multiple-mode formula are shown to provide much better agreement with experimental data than the previous single-mode curves.

Sources of error are evaluated in the measurement technique for high-dielectric-constant samples. It is shown that the circular-waveguide dielectrometer has a typical maximum error of ± 0.6 percent and probable error of ± 0.25 percent, while the radial-waveguide dielectrometer has typically ± 0.42 percent maximum error and ± 0.17 percent probable error. An order-of-magnitude improvement in accuracy appears feasible, but is not needed in this program. The radial-waveguide dielectrometer has been used to obtain data on the new USAERDL cold pressed TiO_2 ceramic samples and on several samples cut from a single tile of Eccoceram Hi-K90 material. Dielectric constant versus temperature was also measured for four different groups of TiO_2 materials. The temperature coefficients ranged from -65 to -1655 ppm/ $^{\circ}C$. These values are higher than the nominal value of -800 for TiO_2 ceramic.

The previous unloaded-Q measurement technique was improved in several minor details. Data was taken on three groups of TiO_2 ceramic disks in propagating WR-284 waveguide. The best values were

obtained with the USAERDL cold-pressed high-purity samples, with Q_u between 10,000 and 12,000 in the majority of pieces tested. One of these pieces was then used to determine the effect of metal-wall losses by repeating the Q_u measurements in a series of "cut-off" square waveguides having internal dimensions ranging from 1.25 by 1.25 inch to 0.430 by 0.430 inch. In the latter case, the 0.430-inch-diameter disk was tangent to the top and bottom walls of the waveguide. Despite the extremely close proximity, the unloaded Q was diminished only to 5250 in the presence of the silver-plated walls. Resonant-frequency data versus the dimension of the square waveguide are also given.

Frequency-response data are shown for several two-resonator band-pass filters adjusted for maximally flat performance. The bandwidth and center-frequency dissipation loss agree quite well with previously obtained coupling-coefficient and unloaded- Q values.

SECTION III

CONFERENCES

On 20 May 1964, a conference was held to discuss third-quarter progress and plans for the fourth quarter. The location of the conference was the International Hotel at Idlewild, L. I., N. Y., where the 1964 PTGMTT Symposium was being held. The conference was attended by Messrs. J. Agrios, N. Lipetz, and E. A. Mariani of USAERDL, and Dr. S. B. Cohn of Rantec Corp. Draft material for the Third Quarterly Report was reviewed and suggestions were made for further items of investigation.

SECTION III

CONFERENCES

On 20 May 1964, a conference was held to discuss third-quarter progress and plans for the fourth quarter. The location of the conference was the International Hotel at Idlewild, L. I., N. Y., where the 1964 PTGMTT Symposium was being held. The conference was attended by Messrs. J. Agrios, N. Lipetz, and E. A. Mariani of USAERDL, and Dr. S. B. Cohn of Rantec Corp. Draft material for the Third Quarterly Report was reviewed and suggestions were made on further items of investigation.

SECTION IV

FACTUAL DATA

1. Introduction

The First Quarterly Report discusses the nature of dielectric resonators and describes how such resonators may be used in micro-wave filters. The introduction to that report should be consulted for background information, and for a discussion of problems to be solved before dielectric resonators can be used in practice.

In the Second Quarterly Report, an analysis was given of coupling between dielectric resonators spaced along the centerline of rectangular waveguide below cutoff. The resulting formula for coupling coefficient was found to agree with experimental data within about ± 10 percent when the center-to-center spacings exceeded about three quarters of the larger of the two waveguide cross-section dimensions. The deviation for smaller spacings was attributed to the use of only the TE_{10} mode in the analysis. In the present report, the theory is extended to all TE and TM modes excited by the resonators. The new multimode formula is shown to yield theoretical curves agreeing very well with the previous experimental points even when the resonant disks are in contact with each other. Based on this excellent verification, the new formula is concluded to have sufficient accuracy for ordinary design purposes.

Two techniques were described in the Second Quarterly Report for measurements on high dielectric-constant materials. Both techniques utilize geometries such that minor airgaps between the surfaces of the cylindrical samples and adjacent metal walls have negligible effect on measured dielectric-constant values. In order to complete the treatment of these new methods, computations of typical errors

have been made and are discussed in this report. Accuracies on the order of one-half percent are shown to be easily obtained. Measured data on several groups of TiO_2 samples are given.

The method of unloaded-Q measurement presented in the First Quarterly Report is susceptible to major error if the input signal has appreciable frequency modulation. Because the signal source was internally square-wave modulated at 1000 cps, it was suspected that incidental frequency modulation might have affected the accuracy of the measured values. In order to eliminate this possible source of error, an isolator and diode modulator were placed between the signal source and the input of the test setup. This permitted the signal source to be operated with CW output, ensuring absence of any significant frequency deviation. Experimental results were found to agree quite well with the data included in the First Quarterly Report, thus showing that frequency modulation had not appreciably affected the previous measurements. Additional measurements were then made on several groups of samples and on a single sample in a series of waveguides of varying cross sections. The latter data reveals the effect of metal-wall proximity on both Q_u and Γ_0 .

In order to determine the validity of the coupling coefficient and Q_u data, several two-resonator band-pass filters were made having maximally flat response. Reasonably good agreement was obtained between actual and predicted bandwidth and dissipation loss.

2. Coupling Between Dielectric Resonators - Higher Modes

In the Second Quarterly Report¹, a formula was derived for the coupling coefficient between a pair of dielectric-disk resonators spaced along the centerline of a rectangular waveguide below cutoff (Figure 2-1). Good agreement was found between computed curves and

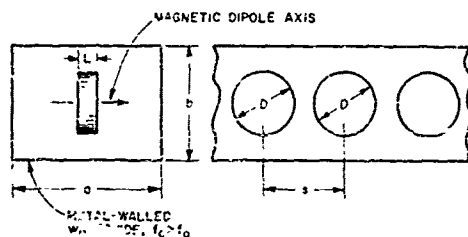


Figure 2-1. Coupled Dielectric Resonators Inside a Rectangular Metal Tube

experimental data when the center-to-center spacing, s , is at least three-fourths of the larger of the two waveguide dimensions, a and b . The discrepancy for closer spacing was attributed to the fact that only the TE_{10} mode was used in the analysis. During the past quarter the treatment was extended to include higher modes.

Considerable improvement in accuracy for close spacing was achieved.

Equation 3-36 of the Second Quarterly Report gives the coupling coefficient, k , in generalized form for a pair of identical magnetic dipole resonators whose axes are either parallel or colinear:

$$k = \frac{\mu_0 \underline{m}_1 \cdot \underline{H}_2}{2W_{m1}} \quad (2-1)$$

where μ_0 is the permeability of free space, \underline{m}_1 and W_{m1} are the magnetic dipole moment and stored energy of the first resonator, while \underline{H}_2 is the magnetic field at the center of the second resonator due to \underline{m}_1 .

In the Second Quarterly Report, \underline{H}_2 was computed from \underline{m}_1 by first determining the amplitude of the TE_{10} mode excited by \underline{m}_1 , then evaluating the magnetic-field amplitude of this mode at a distance s from \underline{m}_1 . The configuration is as shown in Figure 2-1. Because the waveguide is used below its cut-off frequency, the field amplitude is proportional to $e^{-\alpha s}$, where α is the attenuation constant of the TE_{10} mode. Therefore, k is also proportional to $e^{-\alpha s}$, and the theoretical coupling-coefficient curve is a straight line on a semi-log graph. The experimental data showed this to be a good approximation for s relatively large, but not for s relatively small. An improvement in the

latter case may be expected from the addition of higher modes to the coupling analysis.

Consider Figure 2-1. Equation 2-1 indicates that all modes having H_x not zero at the center of the cross section will contribute to the total field H_2 . The significant modes are as follows:

TE_{10}	TE_{12}	TM_{12}
TE_{30}	TE_{32}	TM_{32}
TE_{50}	TE_{52}	TM_{52}
etc.	etc.	etc.

Note that for both TE_{mn} and TM_{mn} , the admissible m and n values are $m = \text{odd integers}$ and $n = \text{even integers}$.

In the Second Quarterly Report, the waveguide-mode notation of Collin² was introduced. The following formulas from pp. 28-30 of the Second Quarterly Report are needed. The MKS system of units are used throughout the analysis.

$$H_2 = H_x^+ \quad \text{at} \quad z = a \quad (2-2)$$

$$H_x^+ = \sum_{m,n} a_{mn} h_{xmn} e^{-\gamma_{mn} z} \quad (2-3)$$

$$a_{mn} = -j \frac{\omega \mu_0}{2} h_{xmn} m_1 \quad (2-4)$$

where m_1 is the moment of the magnetic dipole located at $z = 0$ and directed along the x -axis. The mode field functions e_{mn} and h_{mn} are normalized according to the following power-flow relationship:

$$\iint_S e_{mn} \times h_{mn} \cdot d\mathbf{S} = 1 \quad (2-5)$$

where the integration is performed over the waveguide cross-sectional area. The attenuation constant α_{mn} is given by

$$\alpha_{mn} = \frac{2\pi}{\lambda_{cmn}} \sqrt{1 - \left(\frac{\lambda_{cmn}}{\lambda}\right)^2} \text{ nepers per meter} \quad (2-6)$$

and the cut-off wavelength λ_{cmn} is as follows for rectangular waveguide.

$$\lambda_{cmn} = \frac{i}{\sqrt{\left(\frac{m}{2a}\right)^2 + \left(\frac{n}{2b}\right)^2}} \quad (2-7)$$

Equations 2-2 through 2-7 apply to both TE and TM modes, and the summation in Equation 2-3 is carried out over TE and TM modes of all admissible orders m and n.

When Eqs. 2-2, 2-3, and 2-4 are combined, the following formula for H_2 is obtained.

$$H_2 = -\frac{j\omega\mu_0 m_1}{2} \sum_{m,n} h_{xmn}^2 e^{-\alpha_{mn} s} \quad (2-8)$$

The normalized field component, h_{xmn} , will now be computed. Equation 2-5 can be rewritten with the aid of the relation $\underline{e} \times \underline{h} = d\underline{S}$:
 $\int_S h_t^2 dS = Z (h_x^2 + h_y^2) dS$:

$$Z_{mn} \left[\iint_S h_{xmn}^2 dS + \iint_S h_{ymn}^2 dS \right] = 1 \quad (2-9)$$

where h_{xmn} and h_{ymn} are the transverse components of \underline{h}_{mn} , and the characteristic wave impedance Z_{mn} is as follows:

$$Z_{mn} = \frac{\eta \lambda}{g} = \frac{j2\pi\eta}{\alpha_{mn}} \text{ for TE modes} \quad (2-10)$$

$$Z_{mn} = \frac{\eta \lambda}{g} = \frac{\alpha_{mn} \lambda \eta}{j2\pi} \text{ for TM modes} \quad (2-11)$$

The free-space wave impedance, η , is equal to $\sqrt{\mu_0/\epsilon_0} = 377$ ohms in air.

The h_x and h_y field components are³

$$\left. \begin{aligned} h_{xmn} &= \frac{m}{a} A_{mn} \sin \frac{m\pi x}{a} \cos \frac{n\pi y}{b} \\ h_{ymn} &= \frac{n}{b} A_{mn} \cos \frac{m\pi x}{a} \sin \frac{n\pi y}{b} \end{aligned} \right\} \text{TE}_{mn} \text{ modes} \quad (2-12)$$

$$(2-13)$$

and

$$\left. \begin{aligned} h_{xmn} &= \frac{n}{b} B_{mn} \sin \frac{m\pi x}{a} \cos \frac{n\pi y}{b} \\ h_{ymn} &= -\frac{m}{a} B_{mn} \cos \frac{m\pi x}{a} \sin \frac{n\pi y}{b} \end{aligned} \right\} \text{TM}_{mn} \text{ modes} \quad (2-14)$$

$$(2-15)$$

where A_{mn} and B_{mn} are constants to be evaluated through application of Eq. 2-9. The coordinate system is as shown in Figure 2-2. When

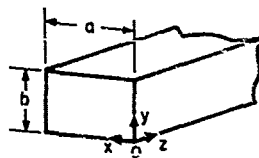


Figure 2-2. Coordinate System for Rectangular Waveguide

Eqs. 2-12 to 2-15 are substituted in Eq. 2-9, the following integrals must be evaluated:

$$\begin{aligned}
\int_0^b \int_0^a \sin^2 \left(\frac{m\pi x}{a} \right) \cos^2 \left(\frac{n\pi y}{b} \right) dx dy &= \int_0^a \sin^2 \left(\frac{m\pi x}{a} \right) dx \int_0^b \cos^2 \left(\frac{n\pi y}{b} \right) dy \\
&= \frac{ab}{4} \text{ for } m \geq 1, n \geq 1 \\
&= \frac{ab}{2} \text{ for } m \geq 1, n = 0
\end{aligned} \tag{2-16}$$

and

$$\begin{aligned}
\int_0^b \int_0^a \cos^2 \left(\frac{m\pi x}{a} \right) \sin^2 \left(\frac{n\pi y}{b} \right) dx dy &= \int_0^a \cos^2 \left(\frac{m\pi x}{a} \right) dx \int_0^b \sin^2 \left(\frac{n\pi y}{b} \right) dy \\
&= \frac{ab}{4} \text{ for } m \geq 1, n \geq 1 \\
&= 0 \text{ for } m \geq 1, n = 0
\end{aligned} \tag{2-17}$$

Equations 2-9, 2-10, 2-12, 2-13, 2-16, and 2-17 yield the following for TE_{m0} modes, $m \geq 1$:

$$\left(\frac{mA_{m0}}{a} \right)^2 = \left(\frac{2}{ab} \right) \left(\frac{a_{m0}^2}{j2\pi\eta} \right) \tag{2-18}$$

$$h_{xm0}^2 = \frac{a_{m0}^2}{jab\pi\eta} \sin^2 \left(\frac{m\pi x}{a} \right) \tag{2-19}$$

and for TE_{mn} modes, $m, n \geq 1$.

$$\left[\left(\frac{m}{a} \right)^2 + \left(\frac{n}{b} \right)^2 \right] A_{mn}^2 = \left(\frac{4}{ab} \right) \left(\frac{a_{mn}^2}{j2\pi\eta} \right) \tag{2-20}$$

$$h_{xmn}^2 = \left(\frac{2(m/a)^2}{(m/a)^2 + (n/b)^2} \right) \left(\frac{a_{mn}^2}{jab\pi\eta} \right) \sin^2 \left(\frac{m\pi x}{a} \right) \cos^2 \left(\frac{n\pi y}{b} \right) \tag{2-21}$$

Similarly, Eqs. 2-9, 2-11, 2-14, 2-15, 2-16, and 2-17, give the following for TM_{mn} modes, $m, n \geq 1$:

$$\left[\left(\frac{m}{a} \right)^2 + \left(\frac{n}{b} \right)^2 \right] B_{mn}^2 = \left(\frac{4}{ab} \right) \left(\frac{j2\pi}{\alpha_{mn} \lambda \eta} \right) \quad (2-22)$$

$$h_{xmn}^2 = \left(\frac{z(n/b)^2}{(m/a)^2 + (n/b)^2} \right) \left(\frac{j4\pi/ab}{\alpha_{mn} \lambda \eta} \right) \sin^2 \left(\frac{m\pi x}{a} \right) \cos^2 \left(\frac{n\pi y}{b} \right) \quad (2-23)$$

Note that for TM_{mn} modes, neither m nor n can be zero in the rectangular-waveguide case.

Examination of Eqs. 2-19, 2-21, and 2-23 shows that at the center of the cross section $h_{xmn}^2 = 0$ if either $m = \text{even integer}$ or $n = \text{odd integer}$. Thus only modes for which $m = \text{odd integer}$ and $n = \text{even integer}$ will contribute to the coupling when the x -directed magnetic dipoles are placed along the central longitudinal axis of the waveguide.

When Eqs. 2-19, 2-21, and 2-23 are substituted in Eq. 2-8, we obtain

$$H_2 = -\frac{m_1}{ab} \left[\sum_m \alpha_{m0} e^{-\alpha_{m0} z} + 2 \sum_{m,n} \frac{(m/a)^2 \alpha_{mn} e^{-\alpha_{mn} z}}{(m/a)^2 + (n/b)^2} - \frac{8\pi^2}{\lambda^2} \sum_{m,n} \frac{(n/b)^2 e^{-\alpha_{mn} z}}{[(m/a)^2 + (n/b)^2] \alpha_{mn}} \right] \quad (2-24)$$

where the summations are performed for $m = 1, 3, 5, \dots$ and $n = 2, 4, 6, \dots$. Use was made of the identity $\omega \mu_0 \lambda = 2\pi\eta$. The three terms in the brackets are due to the TE_{m0} , TE_{mn} , and TM_{mn} modes, respectively. A simplification may be made by observing that Eqs. 2-6 and 2-7 lead to

$$\left(\frac{m}{a}\right)^2 \alpha_{mn} - \left(\frac{2\pi}{\lambda}\right)^2 \left(\frac{n}{b}\right)^2 \left(\frac{1}{\alpha_{mn}}\right) = \left[\left(\frac{m}{a}\right)^2 + \left(\frac{n}{b}\right)^2\right] \frac{\alpha_{m0}^2}{\alpha_{mn}} \quad (2-25)$$

thus,

$$H_2 = -\frac{m_1}{ab} \left[\sum_m \alpha_{m0} e^{-\alpha_{m0}s} + 2 \sum_{m,n} \frac{\alpha_{m0}^2}{\alpha_{mn}} e^{-\alpha_{mn}s} \right] \quad (2-26)$$

where $m = 1, 3, 5, \dots$ and $n = 2, 4, 6, \dots$

A further simplification gives the following compact result.

$$H_2 = -\frac{m_1}{ab} \left[\sum_{m,n} \frac{\alpha_{m0}^2}{\alpha_{mn}} e^{-\alpha_{mn}s} \right] \quad (2-27)$$

In this particular case, the double summation is carried out over $m = 1, 3, 5, \dots, \infty$, and $n = -\infty, \dots, -6, -4, -2, 0, 2, 4, 6, \dots, \infty$. However, Eq. 2-26 in terms of positive integers is more convenient for computation.

The coupling coefficient between a pair of identical x-directed magnetic dipoles on the central longitudinal axis of a rectangular waveguide below cutoff is obtained from Eqs. 2-1 and 2-26.

$$k = \frac{1}{ab} \left(\frac{\mu_0 m_1^2}{2W_{m1}} \right) \left[\sum_m \alpha_{m0} e^{-\alpha_{m0}s} + 2 \sum_{m,n} \frac{\alpha_{m0}^2}{\alpha_{mn}} e^{-\alpha_{mn}s} \right] \quad (2-28)$$

The factor $\mu_0 m_1^2 / 2W_{m1}$ depends only on the dimensions D and L , dielectric constant, ϵ_r , and resonant wavelength, λ_0 of the electric resonator. In the Second Quarterly Report, Fig. 3-52, this factor was evaluated to be

$$\frac{\mu_0 m_1^2}{2W_{m1}} = \frac{0.927 D^4 L \epsilon_r}{\lambda_0^2}, \quad 0.25 \leq L/D \leq 0.7 \quad (2-29)$$

Equation 2-29 was simplified from a more complicated expression given in Eq. 3-51 of the Second Quarterly Report. In the range $0.25 \leq L/D \leq 0.7$ the two formulas agree within $\pm 2\%$. A dielectric resonator of practical proportions will generally lie in this range. Thus,

$$k = \frac{0.927 D^4 L \epsilon_r}{ab \lambda_0^2} \left[\sum_{m,0} \alpha_{m0} e^{-\alpha_{m0}s} + 2 \sum_{m,n} \frac{\alpha_{m0}^2}{\alpha_{mn}} e^{-\alpha_{mn}s} \right] \quad (2-30)$$

where

$$0.25 \leq L/D \leq 0.7$$

$$m = 1, 3, 5, \dots$$

$$n = 2, 4, 6, \dots$$

If L/D falls outside of the range 0.25 to 0.7, the curve plotted in Figure 3-5 of the Second Quarterly Report may be applied as a correction factor to Eq. 2-30.

An interesting property of Eq. 2-24 is that the third summation term, arising from the TM_{mn} modes, is opposite in sign to the TE_{m0} and TE_{mn} terms. The explanation for this difference in sign is as follows. An x-directed magnetic dipole in free space produces an electric field having only y and z components. Thus E_x is everywhere zero. An x-directed magnetic dipole in a rectangular waveguide is equivalent to a two-dimensional infinite array of x-directed dipoles in free space. Since $E_x = 0$ for each dipole, E_x is zero for the superposition of fields of all the dipoles in the array. Hence, only E_y and E_z components exist in the waveguide and E_x is everywhere zero. The field produced by each individual TE_{mn} and TM_{mn} mode (m and $n \geq 1$) contains finite E_x components. However, when the TE_{mn} and TM_{mn} mode fields have the relative amplitudes A_{mn} and B_{mn} determined from Eqs. 2-20 and 2-22, the E_x components of these modes are equal in amplitude and opposite in sign for each set of integers m and $n \geq 1$.

Consequently, the above solution conforms to the necessary condition that $E_x = 0$ at all points in the waveguide.

When only the $m = 1$ term of the first summation is used and the second summation is omitted entirely, the single-mode formula in the Second Quarterly Report is obtained as follows:

$$k = \frac{0.927D^4 L \epsilon_r \alpha_{10} e^{-\alpha_{10}s}}{ab\lambda_0^2} \quad (2-31)$$

Thus, the correction factor

$$K = \frac{1}{\alpha_{10} e^{-\alpha_{10}s}} \left\{ \sum_m \alpha_{m0} e^{-\alpha_{m0}s} + 2 \sum_{m,n} \frac{\alpha_{m0}^2}{\alpha_{mn}} e^{-\alpha_{mn}s} \right\} \quad (2-32)$$

$$m = 1, 3, 5, \dots$$

$$n = 2, 4, 6, \dots$$

converts the single mode formula Eq. 2-31 into the multi-mode formula Eq. 2-30. The factor, K , may be used to correct the computed curves in the Second Quarterly Report for the effects of higher modes. This has been done, and the results are described below.

Application of Correction Factor to Previous Data

In the Second Quarterly Report, three rectangular guide sizes were used in obtaining experimental coupling data. The sizes are $a = b = 0.750$ in., $a = b = 0.995$ in., and $a = 0.625$ in., $b = 1.374$ in. In each waveguide, two different sizes of dielectric disks were used. However, Eq. 2-32 is a function only of f_0 of the disk, and not of the other disk parameters. Since f_0 is approximately the same for both disks, and K is quite insensitive to changes in f_0 , the f_0 values for

the $D = 0.393$ in. and $L = 0.160$ in. disk will be used, but the resulting K factor will be used for the other disk as well.

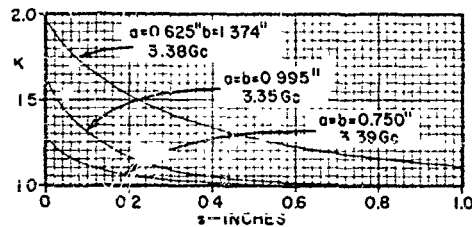


Figure 2-3. Factor K , Ratio of Multiple-Mode Coupling-Coefficient Formula to Single-Mode Formula

correction factor K versus s appears in Figure 2-3 for the three different waveguides.

Figure 2-4 shows the six sets of coupling data from the Second Quarterly Report. The solid curves are theoretical for single-mode coupling, while the dotted curves include the higher-mode contribution, as given by Eqs. 2-30 and 2-32. A substantial improvement in accuracy is evident when the higher-mode terms are added to the single-mode formula.

3. Dielectric-Constant Measurements

a. Measurement Error with the Circular-waveguide Dielectrometer

The circular waveguide dielectrometer was described in the Second Quarterly Report.¹ The device was shown to offer good precision in determining the dielectric constant of materials. An especially important feature of this technique is that it is unaffected by small air gaps between the sample under test and the adjacent

For the square waveguides, calculations show that significant contributions to the coupling coefficient are made only by the modes with subscripts $mn = 10, 30, 50, 12, 14, 32, 34$. For the rectangular waveguide the significant subscripts are $10, 30, 12, 14, 16, 32, 34, 36$. A graph of the

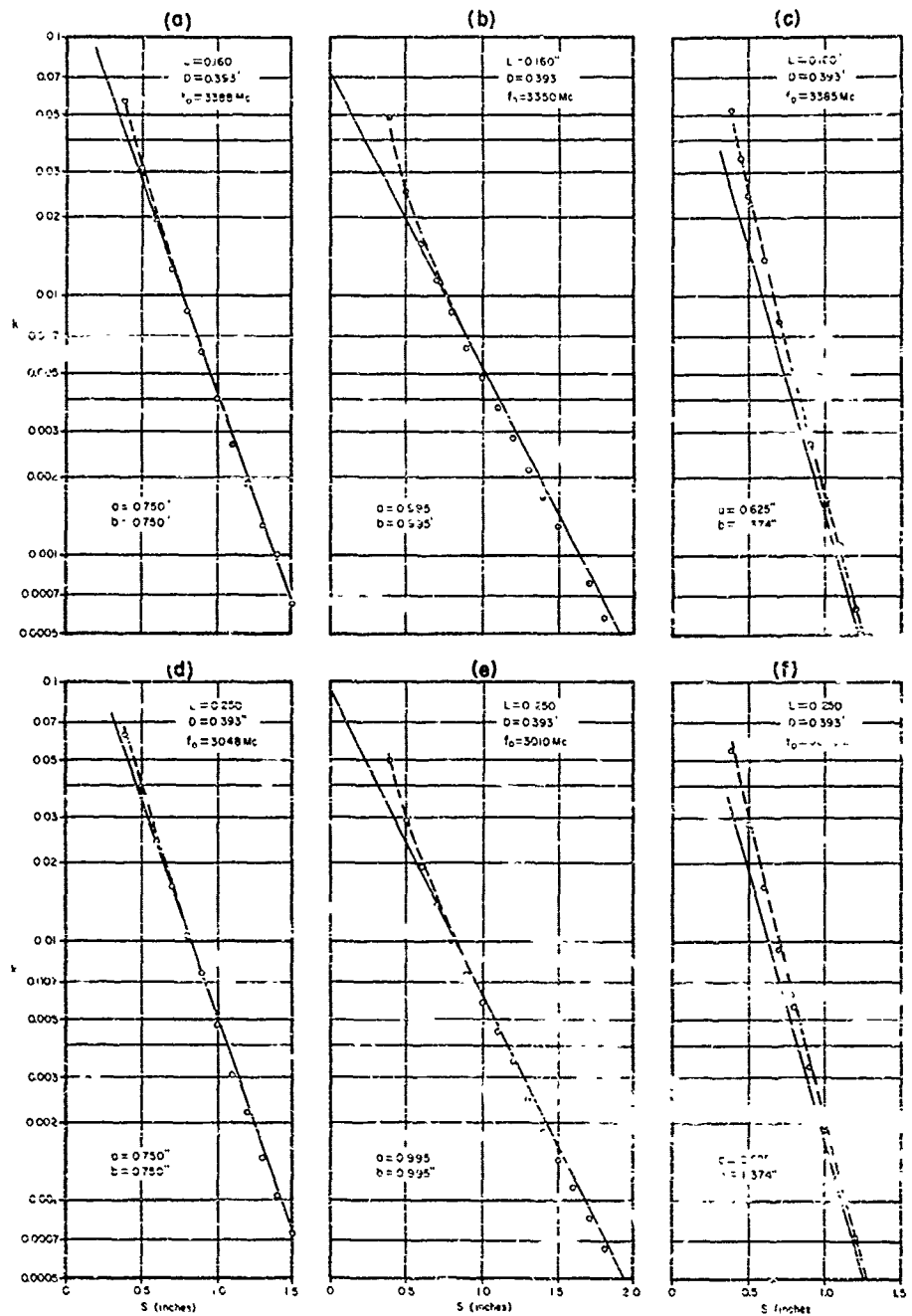


Figure 2-4. Coupling-Coefficient Data for Configuration of Figure 2-1. Solid Curves from Single-Mode Theory, Dotted Curve from Multi-Mode Theory, and Circled Points are Experimental

metal wall. As a result, the technique is particularly useful in measurements on high dielectric-constant materials, where small air gaps are ordinarily a major source of error. The dielectric constant is calculable from the TE_{01} -mode resonance of a right-circular cylinder of the material closely fitted in a below-cutoff metal tube. As indicated in the discussion in the Second Quarterly Report, the computation of dielectric constant, ϵ_r , requires knowledge of the resonant frequency, the inside diameter of the tube, and the length of the sample.

The resonant frequency can easily be measured to 0.1 percent and linear dimensions of the sample to ± 0.0005 inch. As a typical example, a sample was assumed with a dielectric constant of 90.000, a diameter of 0.36000 in., and a length of 0.11800 in. The calculated resonant wavelength of this sample in an ideal circular waveguide dielectrometer is 2.2598 in. When the wavelength, diameter, and height are deliberately offset by -0.1 percent, +0.0005 in., and +0.0005 in., respectively, the dielectric constant is calculated to be $\epsilon_r = 89.43$, which is 0.6 percent low. Note that the errors in the three input quantities were taken with a "worst case" combination of algebraic signs to give the maximum error in ϵ_r . With more precise instruments, the frequency and dimensions can be determined with an order-of-magnitude improvement, so that an accuracy in ϵ_r of better than 0.06 percent appears feasible.

The range of dielectric constants and sample sizes being measured in this program generally conform to the hypothetical case considered above. Thus, in the measurements made with the circular-waveguide dielectrometer, the maximum error in the determination of ϵ_r is less than ± 0.6 percent, and the probable error is about ± 0.25 percent.

b. Measurement Error with the Radial-Waveguide Dielectrometer

The radial-waveguide dielectrometer described in the Second Quarterly Report was also examined from the standpoint of maximum-possible error. The sample employed in the analysis was equivalent, essentially, to the smallest-diameter samples (such as Sample A₃) of the Second Quarterly Report. These smaller samples are nominal 1/4-in. in diameter by 1/10-in. long, with $\epsilon_r = 86.5$.

A numerical error computation was performed assuming the same wavelength and dimension errors as above. The maximum possible error in ϵ_r was found to be ± 0.42 percent while the probable error would be about ± 0.17 percent. Again, order of magnitude improvements of accuracy in frequency and dimensions, and hence in ϵ_r , are feasible.

c. Anomalous Behavior of Sample A₂

It has been found that compressed polycrystalline TiO₂ ceramics from a given batch produce an ϵ_r versus density curve that is well behaved (smooth and monotonic). Sample A₂ of the group of samples tested and reported in the Second Quarterly Report appeared to violate this concept. Numerous remeasurements of this sample reinforces the reported result that its data points differ by as much as 0.1 percent in opposite directions for the two methods of measurement. These measurements included such refinements as use of a frequency counter to give better than 0.001 percent accuracy in the measurement of resonant frequency.

The only reasonable explanation found for the anomaly depends on the assumption that a marked inhomogeneity exists in the

density of the material within the sample. Note that the electric field is zero on the cylindrical walls of the test sample when it is tested in the circular-waveguide dielectrometer. In the radial-waveguide dielectrometer, the electric field is zero on the parallel faces of the sample. In both cases the resonant mode is designated TE_{01} , but the differences in boundary conditions are such that the inhomogeneities within the sample can have markedly different effects on the resonant frequency for the two field distributions of interest.

Support for the idea of inhomogeneities within a small volume comes from test results on a specimen of *Eucoceram* H5 K20 (TiO_2) to be reported below. A further test of the inhomogeneity theory will be the careful measurement of the unloaded Q of sample A_2 as compared to the Q of a similarly sized sample whose indicated ϵ_r fits the ϵ_r -versus-density curve. Marked inhomogeneities would be expected to lower the unloaded Q since asymmetric inhomogeneities should cause energy transfer from the TE_{01} mode into other modes.

d. The Dielectric Constant of Cold Pressed Polycrystalline TiO_2 Pellets from USAERDL

The hot-pressed pellet of fired polycrystalline TiO_2 identified as S_1 was reported to have a dielectric constant of 97.6 - 98.7 in the Second Quarterly Report. New samples of high-purity polycrystalline TiO_2 have been received from USAERDL. These samples are marked "cold pressed," and various press pressures are indicated. In general, these samples displayed lower dielectric constants than the earlier samples. The relation between dielectric constant and density is evident though no assurance was given that all pellets were formed from the same batch. The dielectric constants were determined with the aid of the radial waveguide dielectrometer. The results are given in Figure 3-1. The density and stated pressing pressures used in the fabrication of the pellets tracked in a general way.

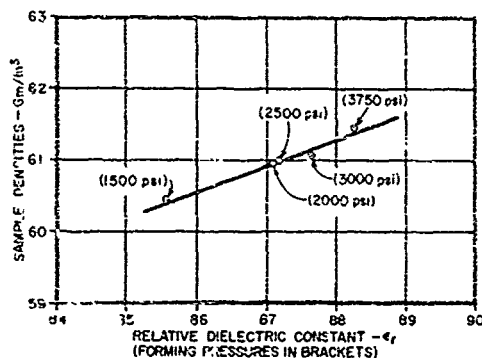


Figure 3-1. Density Vs. Dielectric Constant for US ERDL Cold Pressed TiO_2 Cylinders

e. The Dielectric Constant of Eccoceram Hi-K90

The firm of Emerson and Cuming, Inc. produces and markets a material known as Eccoceram Hi K. The material is said to be polycrystalline TiO_2 , but the company's Technical Bulletin 9-2-5 does not identify the composition. Dissipation factor is given as less than 0.001. The material is available in 12 values of ϵ_r . The Bulletin statement that the material is "usable continuously over the temperature range -70°F to $+1500^\circ\text{F}$ " followed by a listing of dielectric constants implies that ϵ_r was stabilized against temperature. Inquiries failed to produce information on the temperature coefficient associated with ϵ_r .

A single tile, $2\frac{1}{2}$ " by $2\frac{1}{2}$ " by $\frac{3}{8}$ ", of Eccoceram Hi-K90 was obtained for tests. Pellets of 0.340 inch diameter by 0.1180 length were ground from various locations on the tile. The density of the pellets was found to differ by as much as 2 percent. There is no reason to believe that the two-percent figure would not be exceeded if more pellets were made from the remaining portions of the tile. This inhomogeneity within one tile further suggests that the explanation given above for the anomaly observed in Sample A_2 has merit.

One sample, with a density of 63.81 grams/cubic inch, was measured to have a dielectric constant of 91.75. The dielectric constants of the other samples were not measured at this time.

f. Temperature and Dielectric Constant

Four groups of TiO_2 have been measured at a minimum of two temperature, 76°F and 176°F . The results are summarized in Figure 3-2. None of the materials tested show evidence of temper-

ature-compensating ingredients. Because of the high sensitivity of dielectric constant to temperature, it would be generally impractical to construct narrow-band filters for field use out of any of these materials.

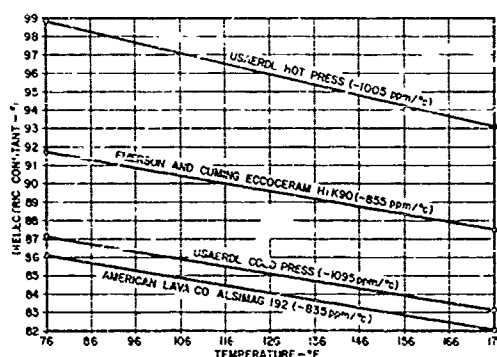


Figure 3-2. Dielectric Constant Vs. Temperature (Temperature Coefficient in Brackets)

4. Unloaded-Q and Center-Frequency Measurements

a. Unloaded Q of TiO_2 Samples

During the third quarter, a series of measurements were made on the unloaded Q, Q_u , of various TiO_2 samples. These samples, which were in the form of cylindrical disks approximately 0.4 inch diameter by 0.2 inch long, were placed at the center of a WR-284 waveguide cross section. As indicated by previous data shown in Table 3-3 of the First Quarterly Report⁴, the metal wall losses in this case would be expected to have negligible effect on Q_u .

The method of Q_u measurement utilized in these tests is essentially as described in the First Quarterly Report. The resonant disk produces a band-rejection response in the operating range of the WR-284 waveguide. By means of a reflectometer setup the rejection bandwidth is determined from reflection-coefficient data. An additional parameter measured is the peak insertion loss of the rejection response. The First Quarterly Report explains how Q_u is computed from bandwidth, center frequency, and peak insertion loss.

Several refinements in technique were introduced in the original equipment shown in the First Quarterly Report. One refinement was the use of an external square-wave diode modulator instead of the internal 1000-cps modulation of the generator. A ferrite isolator was connected between the generator and the diode modulator. This system modification permitted CW operation of the generator, thus eliminating the possibility of frequency modulation as a source of error. A second refinement was the use of a transfer oscillator and counter for precise measurement of frequency. Measurements were repeated on several of the same TiO_2 samples tested during the first quarter. The agreement with the earlier data was very good, indicating that frequency modulation and frequency error had not had a serious effect. However, the use of the isolated external modulator and of the transfer oscillator and counter has been retained because of the greater inherent reliability and precision they afford.

Unloaded Q measurements were made on three sets of TiO_2 samples: (1) hot-pressed samples supplied by the USAERDL ceramics laboratory during the first quarter of this program; (2) cold-pressed samples supplied by the same source during the second quarter; and (3) Eccoceram Hi-K90 material purchased from Emerson and Cuming, Inc. The resulting Q_u values are shown in Table 4-1 with dimensions, center frequencies, and measured dielectric constants.

TABLE 4-1
UNLOADED Q OF VARIOUS TiO₂ CERAMIC DISKS

Material	Identification of Sample	D (inch)	L (inch)	f _o (Mc)	ε _r	Q _u
USAERDL Hot-Pressed	No. 1	0.393	0.750	2980	98	7300
	No. 2	0.393	0.250	2961	98	8530
	No. 3	0.393	0.160	3321	98	7160
	No. 4	0.393	0.160	3317	98	6390
USAERDL Cold-Pressed	1500 psi	0.430	0.220	3051	85.6	12,000
	2000 psi	0.430	0.220	3029	87.1	11,650
	2500 psi	0.540	0.240	2507	87.2	11,700
	3000 psi	0.400	0.200	3289	87.6	7,350
	3750 psi	0.540	0.240	2503	88.2	10,500
	"refired"	0.446	0.244	2675	-	9,350
Eccoceram Hi-K90	No. 1	0.430	0.220	2904	92	7,163
	No. 2	0.430	0.220	2922	91	6,418

b. Q_u Versus Waveguide Dimensions

Figure 4-1 shows the effect of waveguide-wall proximity on the unloaded Q of a dielectric resonator. The resonator used in this experiment is the previously tested USAERDL cold-pressed 2000 psi sample. As shown in Table 4-1, the Q_u value in WR-284 waveguide is 11,650. The plotted points in Figure 4-1 are for this resonator in square waveguides ranging from 0.430 by 0.430 to 1.25 by 1.25 inch ID. The resonator was supported at the center of each waveguide cross section by polyfoam, with the axis of the disk in the transverse x direction. Because the square waveguides are nonpropagating at the resonant frequency of the disk, the configuration was measured as a single-resonator band-pass filter. Coupling loops of closely fitted

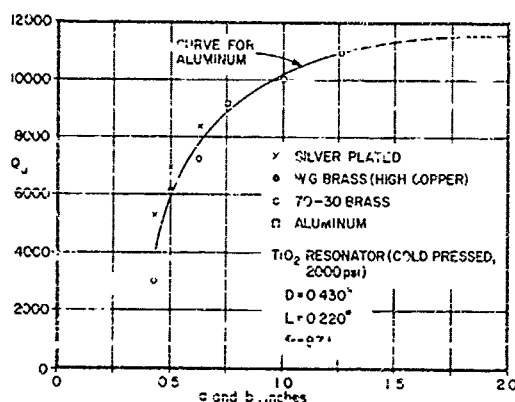


Figure 4-1. Q_u of Dielectric Resonator Vs. Dimension of Square Waveguide

sliding blocks were used to obtain coaxial input and output connections. The loops were adjusted to give a center-frequency insertion loss of at least 3 db. Symmetry of coupling was ensured by setting the loops such that the VSWR at the two ports was the same. The following relationship then holds between loaded Q , Q_L , unloaded Q , Q_u , and center-frequency insertion loss, L_c :⁵

$$L_c = 20 \log_{10} \left(\frac{Q_u}{Q_u - Q_L} \right) \text{ db} \quad (4-1)$$

or

$$Q_u = \frac{Q_L}{1 - 10^{-L_c/20}} \quad (4-2)$$

The loaded Q , Q_L , of the single-resonator filter is related to bandwidth by⁴

$$Q_L = f_o / (BW)_{3\text{db}} \quad (4-3)$$

$$Q_L = \sqrt{3} f_o / (BW)_{6\text{db}} \quad (4-4)$$

$$Q_L = 3 f_o / (BW)_{10\text{db}} \quad (4-5)$$

where $(BW)_{3\text{db}}$, $(BW)_{6\text{db}}$, and $(BW)_{10\text{db}}$ are bandwidths determined at levels of $L_o + 3$ db, $L_o + 6$ db, and $L_o + 10$ db, respectively. These three bandwidths were measured in all cases, and were found to yield sets of Q_L values within about 2 percent of each other. The average

of the Q_L values computed from Eqs. 4-3, 4-4, and 4-5 was used in Eq. 4-2 to obtain Q_u .

The plotted points in Figure 4-1 are for a number of different tubing materials. After the three brass tubes were tested, they were silver plated, thus yielding additional points. The curve in Figure 4-1 applies to aluminum; for cross sections smaller than ~ 75 by 0.75 inch the curve is interpolated between the points for silver-plated and 70-30-brass surfaces.

The Q_u curve in Figure 4-1 is seen to be consistent with an asymptotic value of 11 650 for an "isolated" resonator, as previously measured in 2.84 by 1.34 inch ID waveguide. Although Q_u has dropped to 5250 in silver-plated 0.430 by 0.430 inch tubing, this is nevertheless a highly respectable value. For example, a strip-line or coaxial resonator occupying the same volume would have a Q_u value of about 1200.

The 0.430 by 0.430 inch tubing size is especially interesting, since the 0.430-inch diameter disk is tangent to the top and bottom walls. In this case, a convenient structural technique would be to fasten the disk in place by means of small amounts of epoxy cement at the points of tangency. Another piece of brass tubing was constructed to explore further this possibility. The height was maintained at 0.430 inch to retain the tangency feature, while the width was made 0.860 inch. The unloaded Q in this 70-30-brass tubing was measured to be 5100. After silver plating, Q_u increased to 6760. These values are considerable improvements over the 0.430-inch-square case.

c. f_o Versus Waveguide Dimensions

The effect of waveguide-wall proximity on resonant frequency of the USAERDL 2000 psi cold-pressed sample is shown in

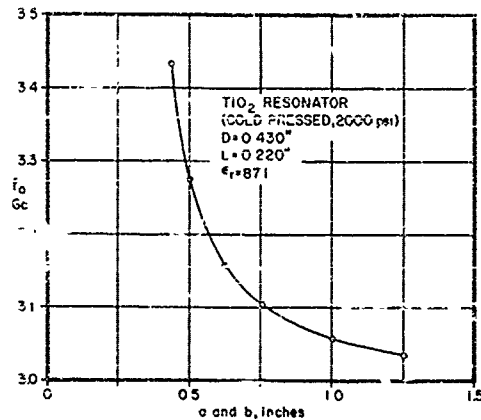


Figure 4-2. f_o of Dielectric Resonator Vs. Dimension of Square Waveguide

Figure 4-2. The measured points are for the same series of square tubings as in the Q_u measurements of Figure 4-1. Table 4-1 shows the resonant frequency of the disk to be 3029 Mc in 2.84 by 1.34 inch waveguide. This asymptotic value is consistent with the curve in Figure 4-2.

In the case of the 0.430 by 0.860 inch tubing, the resonant frequency was measured to be 3234 Mc.

d. Theoretical Analysis of f_o and Q_u

An approximate theoretical analysis of the effect of metal-wall proximity on f_o and Q_u was carried out during the latter part of the third quarter. Initial results of the theory indicate good confirmation of the f_o data in Figure 4-2, and fair confirmation of the Q_u data in Figure 4-1. The theory will be further evaluated, and included in the next report.

e. Experiments with Two-Resonator Band-Pass Filters

In the Second Quarterly Report,¹ coupling data were given for two different pairs of resonators in three different sizes of waveguides

below cutoff. The graphs of experimental points are repeated in the present report as Figure 2-4, where they may be compared with theoretical curves. As an experiment to check the correlation of the data with actual filter performance, the end loops were moved closer to the coupled-resonator pairs in order to produce maximally flat response curves. The results for two cases are shown in Figures 5-1 and 5-2. The pertinent dimensions are indicated in the figures.

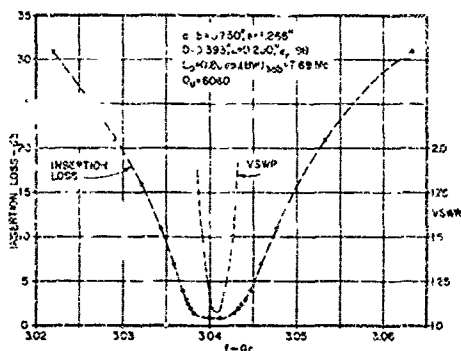


Figure 5-1. Maximally Flat Dielectric-Resonator Filter, $a = b = 0.750''$

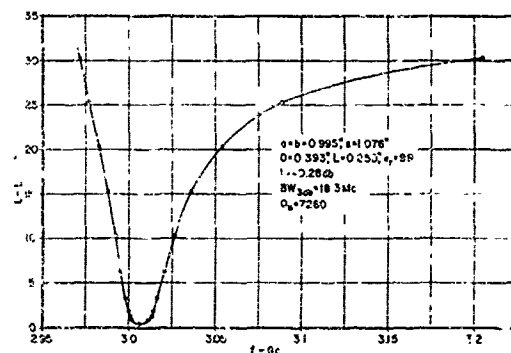


Figure 5-2. Maximally Flat Dielectric-Resonator Filter, $a = b = 0.995''$

The 3-db bandwidth of a two-resonator maximally flat filter is related to the coupling coefficient k_{12} by⁶

$$(BW)_{3db} = \sqrt{2} f_c k_{12}$$

or,

$$k_{12} = 0.707 \frac{(BW)_{3db}}{f_c} \quad (5-2)$$

From the experimental data in Figure 5-1, the coupling coefficient was computed and compared with the previously measured value from

Figure 2-4d. Thus, in Figure 5-1, $(BW)_{3db} = 7.69$ Mc, $f_o = 3040$ Mc, and hence,

$$k_{12} = \frac{0.707 \times 7.69}{3040} = 0.00179$$

This is very close to the value shown in Figure 2-4d, where at $s = 1.266$ inch, $k_{12} = 0.0017$ from the measured points and $k_{12} = 0.00187$ from the theoretical curve.

In Figure 5-2, $(BW)_{3db} = 18.3$ Mc and $f_o = 3030$ Mc. Therefore,

$$k_{12} = \frac{0.707 \times 18.3}{3030} = 0.00427$$

while Figure 2-4e gives $k_{12} = 0.0046$ from the measured points and 0.0050 from the theoretical curve.

A third case that was not plotted had the same parameters as Figure 5-1, except that $s = 1.000$ inch. The coupling coefficient determined from the 3-db bandwidth is 0.00482, while the measured points in Figure 2-4d give 0.0048, and the theoretical curve gives 0.0052.

The resonator unloaded Q values were deduced from the bandwidth and center-frequency dissipation-loss measurements. The relationship for a maximally flat two-resonator filter is as follows:⁷

$$Q_u = \frac{4.34 \times 2.83 f_o}{(BW)_{3db} L_o}$$

where f_o and $(BW)_{3db}$ are in Mc, and L_o is in db. For the three cases discussed above, the Q_u values were found to be 6960, 7260, and 5140, respectively. Note that the second value applies to 0.995 by 0.995 inch tubing, while the other values are for 0.75 by 0.75 inch tubing. In all cases the walls are aluminum.

Both Figure 5-1 and 5-2 indicate a dissymmetrical response. This is especially pronounced in Figure 5-2, where the bandwidth is approximately twice that of Figure 5-1. The possible causes of the observed dissymmetry will be investigated during the next quarter. Techniques of eliminating or reducing this dissymmetry will be explored.

SECTION V

CONCLUSIONS

The new multiple-mode coupling-coefficient formula is vastly superior to the earlier single-mode formula when the dielectric disks are close together. Comparison with experimental points shows good agreement even when the disks are touching each other.

Calculations of errors in the two techniques for dielectric-constant measurement indicate typical precisions of about $\pm 0.5\%$ maximum error and $\pm 0.2\%$ probable error. These values are based on dimensional measurements to ± 0.0005 inch and frequency measurements to ± 0.1 percent. An improvement of accuracy by at least an order of magnitude appears feasible, but is not necessary for the purposes of this program.

Density variations in ceramic samples were previously suspected as the cause of minor anomalies in measured dielectric-constant values. Further confirmation of this possibility was found when various samples cut from a large single piece of TiO_2 ceramic were found to have densities varying by as much as 2 percent. The effect of temperature on dielectric constant was also found to exceed the nominal sensitivity of $-800 \text{ ppm}/^\circ\text{C}$ by amounts ranging from about 5 to 37 percent in four different groups of samples.

The setup for Q_u measurements described in the Final Quarter Report was improved through the use of an isolated external modulator and more precise frequency-measurement equipment. Several of the dielectric pieces previously tested were rechecked and found to agree reasonably well with the earlier data. Therefore, the setup improvements were not found to be essential. Nevertheless they have been retained because of the greater reliability and precision they afford.

Measurements made with this setup show the USAERDL high-purity cold-pressed samples to have considerably higher Q_u than previously obtained TiO_2 batches. Other measurements on a dielectric disk in a series of square waveguides confirm that Q_u is drastically affected when the waveguide dimension is made less than twice the diameter of the disk. However, even when the waveguide dimension was equal to the diameter of the disk, Q_u was approximately 5000 for silver-plated waveguide-walls. This is about four times the Q_u value obtainable in a practical coaxial or strip-line resonator having the same external volume of approximately $0.5 \times 0.5 \times 0.5$ inch.

Experiments on several two-resonator maximally flat filters confirm the validity of the coupling-coefficient and unloaded-Q data previously obtained. A dissymmetry of the stop-band response was observed. This dissymmetry becomes more severe as the filter bandwidth is widened. Since a dissymmetrical response is usually a disadvantage in a bandpass filter, methods of reducing this effect should be found.

SECTION VI
PROGRAM FOR NEXT INTERVAL

The analysis of resonant frequency and coupling will be further developed. The theoretical treatment of metal-wall proximity and its effect on f_o and Q_u will be completed.

Experimental studies will be continued on c_r and Q_u of dielectric samples. In cooperation with the USAERDL Ceramics Laboratory, an effort will be made to obtain a suitable material or combination of materials having relatively low temperature sensitivity.

An investigation will be made of the stop-band-dissymmetry effect observed in relatively wide-band filters. Techniques for reducing this effect will be examined.

Parameters for deliverable filter models will be selected. These filters will then be designed, constructed and tested.

SECTION VII

LIST OF REFERENCES

1. S. B. Cohn and K. C. Kelly, "Investigation of Microwave Dielectric-Resonator Filters," Second Quarterly Report on Contract DA-36-039-AMC-02267(E), 1 October 1963 to 31 December 1963, Rantec Corp., Project No. 31625.
2. R. E. Collin, "Field Theory of Guided Waves," McGraw-Hill, New York, 1960.
3. S. Ramo and J. R. Whinnery, "Fields and Waves in Modern Radio," 2nd Edition, John Wiley and Sons, Inc., New York, 1953.
4. S. B. Cohn and C. W. Chandler, "Investigation of Microwave Dielectric-Resonator Filters," First Quarterly Report on Contract DA-36-039-AMC-02267(E), 1 July 1963 to 30 September 1963, Rantec Corp., Project No. 31625.
5. Radio Research Lab. Staff, "Very High Frequency Techniques," Chap. 28 by S. B. Cohn, McGraw-Hill Book Co., New York, 1947; p. 745.
6. S. B. Cohn, "Direct-Coupled-Resonator Filters," Proc. IRE, Vol. 45, pp. 187-196, February 1957.
7. S. B. Cohn, "Dissipation Loss in Multiple-Coupled-Resonator Filters," Proc. IRE, Vol. 47, pp. 1342-1348, Aug. 1959.

SECTION VII
IDENTIFICATION OF KEY TECHNICAL PERSONNEL

	Hours
Dr. Seymour B. Cohn Specialist	152
Mr. Kenneth C. Kelly Senior Engineer	198
Mr. Richard V. Reed Engineer	237

AD	DIV	UNCLASSIFIED	AD	DIV	UNCLASSIFIED
Rantec Corporation, Calabasas, California	MICROWAVE DIELECTRIC-RESONATOR FILTERS, by S. B. Cohn and K. C. Kelly, an investigation. Third Quarterly Report, 1 January to 31 March 1964, 36p. incl. illus. tables, 7 refs. (rept. no. 3, proj. 31625) (Contract DA-36-039-AMC-02267(E)) uncl.	<ol style="list-style-type: none"> I. Dielectric-Resonator Filters -- Analyses Title: Microwave Dielectric-Resonator Filters II. Cohn, S. B. and Kelly, K. C. III. Rantec Corp., Calabasas, Calif IV. Contract DA 36-039-AMC-02267(E) 	Rantec Corporation, Calabasas, California	MICROWAVE DIELECTRIC-RESONATOR FILTERS, by S. B. Cohn and K. C. Kelly, an investigation. Third Quarterly Report, 1 January to 31 March 1964, 36p. incl. illus. tables, 7 refs. (rept. no. 3, proj. 31625) (Contract DA-36-039-AMC-02267(E)) uncl.	<ol style="list-style-type: none"> I. Dielectric-Resonator Filters -- Analyses Title: Microwave Dielectric-Resonator Filters II. Cohn, S. B. and Kelly, K. C. III. Rantec Corp., Calabasas, Calif IV. Contract DA 36-039-AMC-02267(E)
	The coupling analysis is extended to include higher modes. Curves from the new formula provide greatly improved agreement with measurements.			The coupling analysis is extended to include higher modes. Curves from the new formula provide greatly improved agreement with measurements.	
	Sources of error are evaluated in the two measurement techniques for high- Q samples. Maximum errors are about 0.5			Sources of error are evaluated in the two measurement techniques for high- Q samples. Maximum errors are about 0.5	
	(over)	UNCLASSIFIED		(over)	UNCLASSIFIED
AD	DIV	UNCLASSIFIED	AD	DIV	UNCLASSIFIED
Rantec Corporation, Calabasas, California	MICROWAVE DIELECTRIC-RESONATOR FILTERS, by S. B. Cohn and K. C. Kelly, an investigation. Third Quarterly Report, 1 January to 31 March 1964, 36p. incl. illus. tables, 7 refs. (rept. no. 3, proj. 31625) (Contract DA-36-039-AMC-02267(E)) uncl.	<ol style="list-style-type: none"> I. Dielectric-Resonator Filters -- Analyses Title: Microwave Dielectric-Resonator Filters II. Cohn, S. B. and Kelly, K. C. III. Rantec Corp., Calabasas, Calif IV. Contract DA 36-039-AMC-02267(E) 	Rantec Corporation, Calabasas, California	MICROWAVE DIELECTRIC-RESONATOR FILTERS, by S. B. Cohn and K. C. Kelly, an investigation. Third Quarterly Report, 1 January to 31 March 1964, 36p. incl. illus. tables, 7 refs. (rept. no. 3, proj. 31625) (Contract DA-36-039-AMC-02267(E)) uncl.	<ol style="list-style-type: none"> I. Dielectric-Resonator Filters -- Analyses Title: Microwave Dielectric-Resonator Filters II. Cohn, S. B. and Kelly, K. C. III. Rantec Corp., Calabasas, Calif IV. Contract DA 36-039-AMC-02267(E)
	The coupling analysis is extended to include higher modes. Curves from the new formula provide greatly improved agreement with measurements.			The coupling analysis is extended to include higher modes. Curves from the new formula provide greatly improved agreement with measurements.	
	Sources of error are evaluated in the two measurement techniques for high- Q samples. Maximum errors are about 0.5			Sources of error are evaluated in the two measurement techniques for high- Q samples. Maximum errors are about 0.5	
	(over)	UNCLASSIFIED		(over)	UNCLASSIFIED

AD	DIV	UNCLASSIFIED	AD	DIV	UNCLASSIFIED
<p>percent for ϵ_r near 100. Effect of temperature on ϵ_r was measured for four groups of TiO₂ samples. Q_u data were taken on three groups of TiO₂ disks. The best values were obtained with USAERDL cold-pressed high-purity samples, with Q_u between 10,000 and 12,000. One piece was measured in "cut-off" square waveguides of various size. When the disk was tangent to the top and bottom walls, Q_u was diminished only to 5250. Resonant-frequency data versus the dimension of the square waveguide are also given.</p> <p>Response curves are shown for several band-pass filters. Bandwidth and center-frequency loss agree quite well with coupling coefficient and Q_u data.</p>		<p>UNCLASSIFIED</p> <p>UNITERMS</p> <p>Filters</p> <p>Dielectric-Constant Resonator</p> <p>Cylindrical Rectangular</p> <p>Magnetic-Dipole Measurement</p> <p>Microwave Mode</p> <p>Q</p> <p>Coupling Coefficient</p> <p>Stored Energy</p> <p>Temperature Coefficient</p> <p>Bandpass</p> <p>TiO₂</p> <p>UNCLASSIFIED</p>		<p>percent for ϵ_r near 100. Effect of temperature on ϵ_r was measured for four groups of TiO₂ samples. Q_u data were taken on three groups of TiO₂ disks. The best values were obtained with USAERDL cold-pressed high-purity samples, with Q_u between 10,000 and 12,000. One piece was measured in "cut-off" square waveguides of various size. When the disk was tangent to the top and bottom walls, Q_u was diminished only to 5250. Resonant-frequency data versus the dimension of the square waveguide are also given.</p> <p>Response curves are shown for several band-pass filters. Bandwidth and center-frequency loss agree quite well with coupling coefficient and Q_u data.</p>	<p>UNCLASSIFIED</p> <p>UNITERMS</p> <p>Filters</p> <p>Dielectric-Constant Resonator</p> <p>Cylindrical Rectangular</p> <p>Magnetic-Dipole Measurement</p> <p>Microwave Mode</p> <p>Q</p> <p>Coupling Coefficient</p> <p>Stored Energy</p> <p>Temperature Coefficient</p> <p>Bandpass</p> <p>TiO₂</p> <p>UNCLASSIFIED</p>
AD	DIV	UNCLASSIFIED	AD	DIV	UNCLASSIFIED
<p>percent for ϵ_r near 100. Effect of temperature on ϵ_r was measured for four groups of TiO₂ samples. Q_u data were taken on three groups of TiO₂ disks. The best values were obtained with USAERDL cold-pressed high-purity samples, with Q_u between 10,000 and 12,000. One piece was measured in "cut-off" square waveguides of various size. When the disk was tangent to the top and bottom walls, Q_u was diminished only to 5250. Resonant-frequency data versus the dimension of the square waveguide are also given.</p> <p>Response curves are shown for several band-pass filters. Bandwidth and center-frequency loss agree quite well with coupling coefficient and Q_u data.</p>		<p>UNCLASSIFIED</p> <p>UNITERMS</p> <p>Filters</p> <p>Dielectric-Constant Resonator</p> <p>Cylindrical Rectangular</p> <p>Magnetic-Dipole Measurement</p> <p>Microwave Mode</p> <p>Q</p> <p>Coupling Coefficient</p> <p>Stored Energy</p> <p>Temperature Coefficient</p> <p>Bandpass</p> <p>TiO₂</p> <p>UNCLASSIFIED</p>		<p>percent for ϵ_r near 100. Effect of temperature on ϵ_r was measured for four groups of TiO₂ samples. Q_u data were taken on three groups of TiO₂ disks. The best values were obtained with USAERDL cold-pressed high-purity samples, with Q_u between 10,000 and 12,000. One piece was measured in "cut-off" square waveguides of various size. When the disk was tangent to the top and bottom walls, Q_u was diminished only to 5250. Resonant-frequency data versus the dimension of the square waveguide are also given.</p> <p>Response curves are shown for several band-pass filters. Bandwidth and center-frequency loss agree quite well with coupling coefficient and Q_u data.</p>	<p>UNCLASSIFIED</p> <p>UNITERMS</p> <p>Filters</p> <p>Dielectric-Constant Resonator</p> <p>Cylindrical Rectangular</p> <p>Magnetic-Dipole Measurement</p> <p>Microwave Mode</p> <p>Q</p> <p>Coupling Coefficient</p> <p>Stored Energy</p> <p>Temperature Coefficient</p> <p>Bandpass</p> <p>TiO₂</p> <p>UNCLASSIFIED</p>

UNITED STATES ARMY ELECTRONICS RESEARCH & DEVELOPMENT LABORATORIES
STANDARD DISTRIBUTION LIST
RESEARCH AND DEVELOPMENT CONTRACT REPORTS

	<u>Copies</u>
OASD (R & E), Room 3E1065, ATTN: Technical Library, The Pentagon, Washington 25, D. C.	1
Chief of Research and Development, OCS, Department of the Army, Washington 25 D. C.	1
Commanding General, U. S. Army Materiel Command ATTN: R & D Directorate, Washington 25, D. C.	1
Commanding General, U. S. Army Electronics Command ATTN: AMSEI-AD, Fort Monmouth, New Jersey	3
Commander, Defense Documentation Center, ATTN: TISIA Carleton Station, Building 5, Alexandria, Virginia 22314	20
Commanding Officer, U. S. A. Combat Developments Command ATTN: CDCMR-E, Fort Belvoir, Virginia	1
Commanding Officer, U. S. Army Combat Developments Command Communications-Electronics Agency, Fort Huachuca, Arizona	1
Chief, U. S. Army Security Agency, Arlington Hall Station Arlington 12, Virginia	2
Deputy President, U. S. Army Security Agency Board Arlington Hall Station, Arlington 12, Virginia	1
Commanding Officer, Harry Diamond Laboratories, Connecticut Avenue & Van Ness St., N. W., Washington 25, D. C.	1
Director, U. S. Naval Research Laboratory, ATTN: Code 2027 Washington 25, D. C.	1
Commanding Officer and Director, U. S. Navy Electronic Laboratory, San Diego 52, California	1
Aeronautical Systems Division, ATTN: ASNXRR Wright-Patterson Air Force Base, Ohio 45433	1
Air Force Cambridge Research Laboratories, ATTN: CRZC L. G. Hanscom Field, Bedford, Massachusetts	1
Air Force Cambridge Research Laboratories, ATTN: CPKL-R L. G. Hanscom Field, Bedford, Massachusetts	1

	<u>Copies</u>
Hq, Electronic Systems Division, ATTN: ESAT L. G. Hancock Field, Bedford, Massachusetts	1
Rome Air Development Center, ATTN: RAALD Griffiss Air Force Base, New York	1
Advisory Group on Electron Devices, 346 Broadway, 8th Floor, New York, New York 10013	3
AFSC Scientific/Technical Liaison Office, U. S. Naval Air Development Center, Johnsville, Pennsylvania	1
USAEI Liaison Office, Rome Air Development Center, ATTN: RAOL, Griffiss Air Force Base, New York	1
NASA Representative (SAK/DL), Scientific and Technical Information Facility, P. O. Box 5700 Bethesda, Maryland 20014	2
Commander, U. S. Army Research Office (Durham) Box CM - Duke Station, Durham, North Carolina	1
Director of Procurement & Production Directorate ATTN: AMSEL-PP-E-ASD-5, Fort Monmouth, New Jersey	1
Commanding Officer, U. S. Army Engineer Research & Development Laboratories, ATTN: STINFO Branch Fort Belvoir, Virginia 22060	2
Marine Corps Liaison Office, U. S. Army Electronics Laboratories, Fort Monmouth, New Jersey	1
AFSC Scientific/Technical Liaison Office, U. S. Army Electronics Laboratories, Fort Monmouth, New Jersey	1
Commanding Officer, U. S. Army Electronics Laboratories ATTN: AMSEL/RD-DR/DE, Fort Monmouth, New Jersey	1
Director, U. S. Army Electronics Laboratories, ATTN: Technical Documents Center, Fort Monmouth, New Jersey	
Commanding Officer, U. S. Army Electronics Laboratories ATTN: AMSEL-RD-ADO-RHA, Fort Monmouth, New Jersey	1
Commanding Officer, U. S. Army Electronics Research & Development Activity, ATTN: SELWS-A White Sands, New Mexico 88002	1

SUPPLEMENTAL DISTRIBUTION

	<u>Copies</u>
National Bureau of Standards, Engineering Electronics Section ATTN: Mr. Gustave Shapiro, Chief, Washington 25, D. C.	1
Chief, Bureau of Ships, Department of the Navy ATTN: Mr. Cumina, Code 68182, Washington 25, D. C.	1
Commander, Rome Air Development Center, ATTN: Mr. P. Romanel (RCLRA-Z), Griffiss Air Force Base, New York	1
Stanford Research Institute, ATTN: Dr. Matthaei Menlo Park, California	1
Physical Electronic Laboratories, 1185 O'Brien Drive, Menlo Park, California, ATTN: Dr. Carter	1
Stanford Research Institute, Menlo Park, California ATTN: Dr. Young	1
Mr. Robert Standley, Antenna Research Facility I. T. T. Research Institute, Box 205, Geneva, Illinois	1
Mr. Jesse J. Taub, Airborne Instruments Laboratory Deer Park, L.I., New York 11729	1
Professor E. J. Smoke, Rutgers, The State University N. J. Ceramic Research Station, New Brunswick, New Jersey	1
Director, U. S. Army Electronics Laboratories Fort Monmouth, New Jersey	
ATTN: AMSEL-RD-PE (Division Director)	1
ATTN: AMSEL-RD-PE (Dr. E. Roth)	1
ATTN: AMSEL-RD-P (Department Director)	1
ATTN: AMSEL-RD-PEM (Mr. N. Lipetz)	1
ATTN: AMSEL-RD-PEM (Mr. J. Chasman)	1
ATTN: AMSEL-RD-PEM (Mr. E. Mariani)	1